1 Holocene Southwest Greenland Ice Sheet Behavior

2 Constrained by Sea-Level Modeling

- 4 Raf Antwerpen^a, Jacqueline Austermann^a, Nicolás Young^a, David Porter^a, Lauren Lewright^a,
- 5 Konstantin Latychev^b

6

3

- 7 a Lamont-Doherty Earth Observatory, Columbia University, Palisades, NY, USA
- 8 ^b SEAKON, Toronto, ON, Canada
- 9 Corresponding author: Raf Antwerpen (ra3063@columbia.edu)

10

11

Keywords

- 12 Greenland ice sheet, sea level change, glaciation, glacial isostatic adjustment, modeling, Holocene,
- present, tide gauge, GPS

14

15 Abstract

- 16 The melting of the Greenland ice sheet (GrIS) is a major contributor to past and future global sea-
- 17 level rise. Understanding the response of the GrIS to times in the past when temperatures were as
- warm or warmer than today offers insights into its current and future response to climate change.
- 19 In the southwest sector, the GrIS retreated inland beyond its current margin during the (at least
- 20 regionally) warmer-than-present mid-Holocene, before it readvanced to the historical maximum
- 21 position during the Little Ice Age. This was then followed by a slight retreat to its current position.
- 22 To investigate the timing and magnitude of southwest GrIS retreat and readvance in response to

Holocene warmth, we model the response of the solid Earth and local relative sea level (RSL) to past ice sheet change. We test a suite of eleven ice sheet scenarios that are based on ICE-6G_C but are modified in the timing and magnitude of ice retreat and readvance and pair them with four different viscoelastic Earth structures. We compare model predictions to observations of paleo sea level, present-day sea-level change, and present-day vertical land motion (VLM) around Nuuk, Greenland. We find that the modeled timing and magnitude of the Holocene retreat and readvance have a significant impact on modern sea-level change and VLM in Nuuk. Models that assume a readvance approaching the southwest GrIS' historical maximum between 2 and 1 ka are most consistent with observations. The RSL response, however, is less sensitive to the timing of the minimum GrIS extent. Nonetheless, better data-model fits are generally obtained when the minimum ice sheet extent is reached between 5 and 3 ka, within the tested range of 6-3 ka. Comparing this timing to local and regional records of temperature and ice-sheet change suggest that the evolution of the southwestern GrIS presented here was in-phase with the likely evolution of southwestern GrIS mass balance through the Holocene. Our results have implications for future ice sheet modeling studies targeting southwestern Greenland by providing additional constraints and strengthening existing ones. Moreover, this work provides a deeper understanding of the interactions between the climate and the cryosphere and thus of future ice sheet change.

40

41

42

43

44

45

23

24

25

26

27

28

29

30

31

32

33

34

35

36

37

38

39

1. Introduction

Understanding the response of the Greenland ice sheet (GrIS) to a warming climate is crucial for accurately predicting future ice melt and consequent sea-level change. This is particularly pertinent given the projected atmospheric warming in the coming decades, which is amplified in the Arctic (Rantanen et al., 2022; Serreze and Francis, 2006). Reconstructing paleo responses of the GrIS to

similar or warmer climatic conditions than today can aid in understanding future GrIS stability (Fischer et al., 2018).

The most recent period when local temperatures in Greenland were warmer than today is the Holocene Thermal Maximum (HTM; ~7-4 ka) (Briner et al., 2016). During the majority of this time, Greenland's mean summer atmospheric temperature was ~3.3 °C higher than during the 1950 Common Era (CE) (Buizert et al., 2018). Temperatures in the northwest and over the central ice sheet were 3-5 °C higher than in the mid-twentieth century and temperatures in the south were 1-2 °C higher. A reconstructed seasonal temperature record using the Community Climate System Model version 3 and the Summit δ^{15} N temperature reconstruction suggests that the HTM temperatures in Greenland were most pronounced during the summer (Liu et al., 2009; Buizert et al., 2018).

It is widely accepted that the southwestern GrIS region responded to HTM warmth with inland retreat of the ice margin east of its current position (Larsen et al., 2015; Lecavalier et al., 2014; Lesnek et al., 2020; Young et al., 2021, 2020; Young and Briner, 2015). Reconstructing the exact timing and magnitude of the Holocene GrIS minimum, however, remains challenging because direct terrestrial evidence (e.g. moraines) of previous ice sheet minima has since been overrun by ice readvance in the late Holocene. Nonetheless, constraints have been reported on the timing and magnitude of the GrIS minimum by using sediment-based proxies, cosmogenic isotope measurements, and sea-level modeling. A suite of geological constraints suggests that the southwestern GrIS margin had largely retreated behind its present margin by ~7 ka, and likely achieved a minimum extent sometime between ~5-3 ka (Briner et al., 2010; Larsen et al., 2015;

Lesnek et al., 2020; Young et al., 2021, 2020; Young and Briner, 2015). While the precise magnitude of inland retreat is difficult to constrain, these same geological records suggest that inland retreat was likely no more than a few 10s of km and perhaps as little as ≤10 km in some locations (Larsen et al., 2015; Lesnek et al., 2020; Young et al., 2021; Young and Briner, 2015). Following the southwestern GrIS minimum extent, ice-margin readvance culminated in the deposition of the historical moraine ~1850-1900 CE (Weidick et al., 2012; Weidick and Bennike, 2007). Yet, sediment archives from proglacial lakes suggest that the southwestern GrIS may have approached, but not quite reached, the eventual historical maximum ice-margin position as early as ~1-2 ka (Larsen et al., 2015; Pearce et al., 2022; Young et al., 2021). Broadly supporting this ice-margin history is a modeling study that places the southwestern GrIS Holocene minimum extent ~40-60 km inland of its present position at 4 ka (Huy3; Lecavalier et al., 2014). However, the modern ice margin in this reconstruction misses the observed one by several 10s of km, partly due to the coarse 20 km mesh resolution of Huy3. This can lead to physically-inconsistent ice margin dynamics during periods of high ablation as the coarse mesh is not able to resolve the finescale bedrock geometry and the often-narrow ablation zone at the ice margin. In contrast, the ICE-6G_C ice sheet reconstruction exhibits a retreat of ~130-140 km at 6 ka (Argus et al., 2014; Peltier et al., 2015; Stuhne and Peltier, 2015), but does readvance to the correct modern margin. More recently, paleo-benchmarked model runs of southwestern GrIS change through the Holocene using the Ice Sheet and Sea-level System model (ISSM) point to mid-Holocene ice-margin retreat on the order of only a few 10s of km (Briner et al., 2020; Cuzzone et al., 2022; Young et al., 2021). Differences in the magnitude and timing of maximum retreat in ice sheet model-based reconstructions (Huy3 and ISSM) may be driven by differences in the incorporated model physics and resolution. These uncertainties make it difficult to correlate ice sheet behavior with other

69

70

71

72

73

74

75

76

77

78

79

80

81

82

83

84

85

86

87

88

89

90

climate proxies and inhibit understanding the exact response time and sensitivity of the ice sheet to warming.

94

95

96

97

98

99

100

101

102

103

104

105

106

107

108

109

110

111

112

113

92

93

One approach to better understand the past behavior of the GrIS is to study historic and presentday local sea-level variability. Holocene ice sheet changes affect past and present sea-level change due to glacial isostatic adjustment (GIA), which is the response of the viscoelastic solid Earth, its gravity field, and its rotation axis to changes in ice and ocean load. The Holocene retreat and readvance of the southwest GrIS causes a local sea-level curve with a classic "J-shape" where sea level falls to a minimum in response to ice retreat before rising to the modern level (readvance phase), which is characteristic of southwest Greenland (Lecavalier et al., 2014; Long et al., 2011). Further, southwest Greenland is located on the subsiding peripheral bulge of the Laurentide ice sheet (LIS), which causes a superimposed RSL rise (Khan et al., 2016). Additionally, the southwest GrIS briefly advanced and retreated during the Little Ice Age (LIA; ~1450-1900 CE) in response to colder-than-present temperatures. For example, near the Kangiata Nunaata Sermia (KNS) region, the ice sheet reached its maximum historical extent around 1761-1808 CE resulting in the deposition of the so-called historical moraine (Lea et al., 2014; Pearce et al., 2022). The brief advance and retreat cause a contribution to present-day RSL fall due to GIA. In addition to GIA effects, contemporaneous global ice mass changes, changes in water stored on land (Slangen, 2012), thermosteric effects, and ocean dynamics (Levitus et al., 2012) all affect modern sea level change in Greenland. These combined processes lead to a present-day RSL rise in southwest Greenland rather than a RSL fall, as is the case around most of Greenland (Lecavalier et al., 2014; Spada et al., 2014).

Here, we investigate the timing of retreat and readvance of the southwestern GrIS during the Holocene by modeling the GIA effects of different Greenland ice sheet reconstructions on RSL and solid Earth deformation in Nuuk (Figure 1). We compare RSL predictions, driven by a range of retreat and readvance scenarios that are informed by geological constraints of the ice margin position, to paleo sea-level data. We then use the Nuuk tide gauge record and global navigation satellite system (GNSS) observations of modern vertical land motion (VLM) to further test our RSL and VLM predictions during the modern era. This comparison requires a series of corrections related to changes in global ice mass, sterodynamic effects, and changes in terrestrial water mass exchange. This approach allows us to evaluate which Holocene ice retreat and readvance scenario is most consistent with sea-level and GNSS observations.

2. Data and methods

127 2.1 GIA model

We investigate the sea-level response to an evolving global ice and ocean load by solving the sea-level equation using a gravitationally self-consistent GIA model (Kendall et al., 2005). The model is based on a pseudo-spectral approach with a maximum spherical harmonic degree and order of 512 and it accounts for Maxwell viscoelastic solid Earth deformation, gravitational changes of Earth, ice and ocean loading, changes in Earth's rotation axis, and shoreline migration. As input, this model requires a prescribed past ice history and a viscoelastic Earth structure. We run the GIA model with a suite of Earth models and a suite of GrIS reconstructions based on the ICE-6G_C ice model (Peltier et al., 2015).

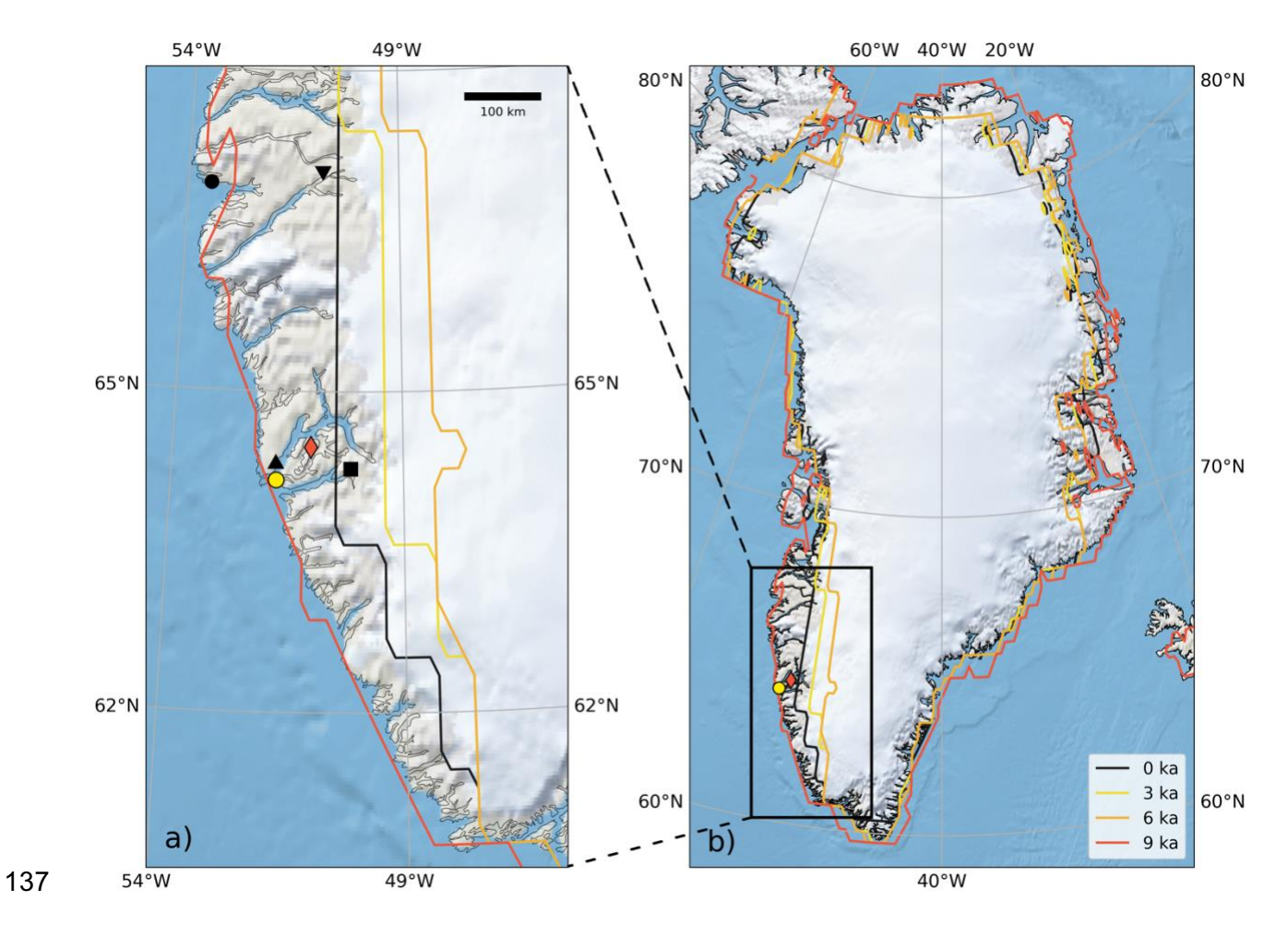


Figure 1: ICE-6G_C ice margin positions (Peltier et al., 2015) for a) southwestern GrIS and b) full GrIS at 9 ka (red), 6 ka (orange), 3 ka (yellow), and present-day (black), at the original resolution with the tide gauge and GPS location in Nuuk (yellow dot; 64.17° N, 51.73° W) and the Nuuk paleo sea-level data location (red diamond; 64.48° N, 50.997° W). Additional paleo sea-level data is shown for Sisimiut (black dot; 66.63° N, 53.64° W), Sondre (black downward triangle; 66.848° N, 50.98° W), Godmouth (black upward triangle; 64.37° N, 51.697° W), and Godhead (black square; 64.434° N, 50.33° W). The modeled ice sheet is coarser than the land margin shown here, which results in some apparent present-day offshore ice margins.

ICE-6G C provides global ice thickness values and follows first-order physical mass balance variations (Argus et al., 2014; Peltier et al., 2015; Stuhne and Peltier, 2015). It is manually adjusted to fit an array of global GPS measurements, time-dependent gravity data from GRACE, and radiocarbon-dated relative sea-level histories. While ICE-6G_C is only an ice model for the deglaciation, a glaciation phase (120-26 ka) has been added to account for any remaining viscoelastic deformation driven by ice change during this time period. To include this phase in the ice history we follow the eustatic curve of Peltier and Fairbanks (2006), assuming that times of equal ice volume follow equal ice geometry. The GrIS component is based on the Gr.B model (Tarasov and Peltier, 2003, 2002). The Holocene ice extent minimum of the southwest GrIS, at the latitude of Nuuk (64.17° N), occurs at 6 ka and the ice margin readvances to a maximum extent by 2 ka (Figure 1), after which it remains stationary. To test how changes in retreat history affect sea-level observations we modify the ice history of the GrIS (and let the other ice sheets follow the original ICE-6G C) to construct a suite of ice scenarios (Figure 2). Exploring later times of ice retreat and readvance is based on the findings by Young et al. (2021) and Pearce et al. (2022), who suggest that the southwest GrIS ice margin minimum likely occurred after ~5 ka and that the ice margin closely approached (but not yet reached) its historical maximum extent by \sim 2 ka or later. Our suite of scenarios include: (1) no retreat and readvance (hereafter referred to as "no retreat"), which is achieved by enforcing a linear change of ice thickness from 8 ka until 2 ka, after which the ice thickness is constant until the present-day. We start the linear change in ice thickness at 8 ka to avoid affecting the RSL curve in the period around the paleo RSL data (section 2.2.1). The ice volume therefore exhibits a minimum at 8 ka in this scenario. There is, however, no ice margin retreat in this scenario; (2) delayed minimum ice extent, where we delay the minimum extent from 6 ka to 5 ka, 4 ka, and 3 ka (3 separate scenarios); and (3) delayed maximum ice extent, where we

147

148

149

150

151

152

153

154

155

156

157

158

159

160

161

162

163

164

165

166

167

168

vary the time of readvance to the maximum extent between 2 ka, 1 ka and present-day (3 separate scenarios). We pair each delayed minimum with each delayed maximum scenario to yield nine different simulations. To modify the timing of ice retreat and readvance we apply a linear adjustment to the rate of GrIS mass change between 8 ka and the timing of the minimum extent to allow for a slower retreat and a later minimum. Similarly, we adjust the rate of change between the subsequent minimum and maximum times accordingly to allow for a later maximum. Adding these nine scenarios to the original ice history and the no retreat and readvance scenario yields eleven different ice histories. We calculate the global sea-level response for each ice reconstruction between 122 ka (last interglacial; LIG) and the present-day (1950 CE), with a temporal resolution of 0.25 kyr during the Holocene and 0.5-2 kyr before the Holocene, following the original resolution of ICE-6G_C.

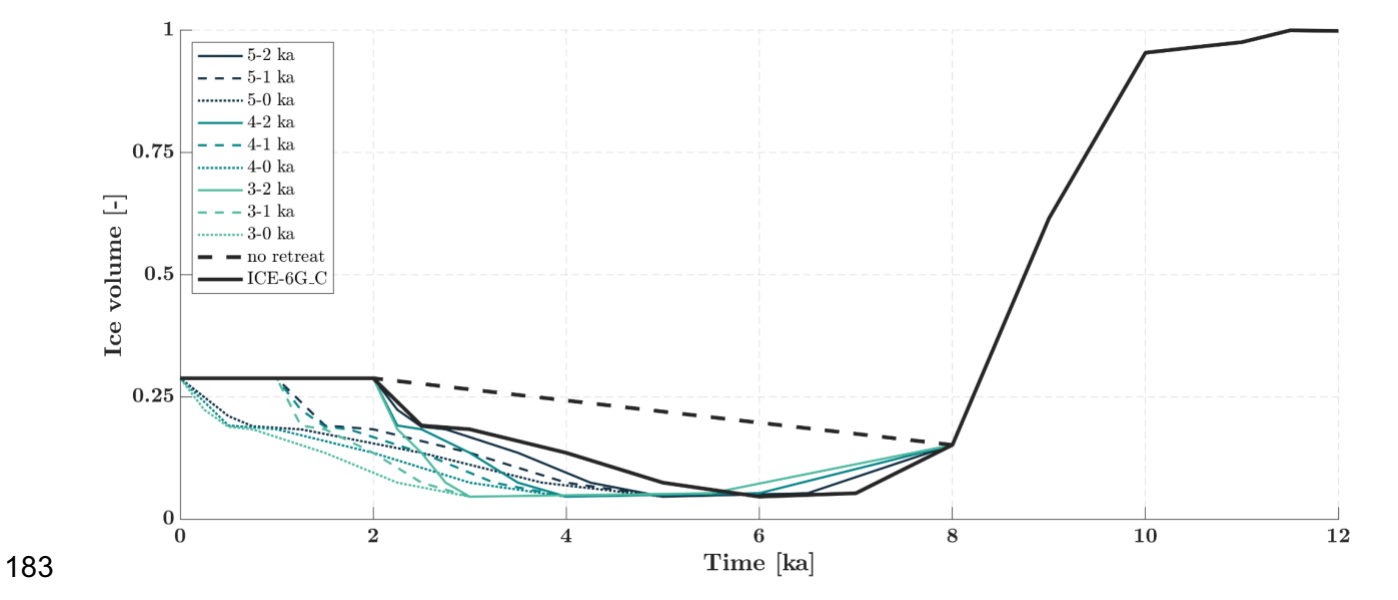


Figure 2: Southwest Greenland ice volume fraction, relative to the ice volume at 12 ka. ICE-6G_C refers to the original ICE-6G_C ice history. Ice histories with adjusted timings are referred to as,

for instance, 5-1 ka, indicating that the Holocene minimum extent is reached at 5 ka and the historical maximum extent is approached at 1 ka.

The Huy3 Greenland ice sheet reconstruction is based on a physical ice sheet model (Lecavalier et al., 2014) and has less retreat and readvance, which is more in line with field observations (Briner et al., 2020; Cuzzone et al., 2022; Young et al., 2021). However, the present-day ice margin in Huy3 near Nuuk is located ~70km west of the observed margin. Contrary to ICE-6G_C, where the observed present-day margin is prescribed in the model. Given the sensitivity of RSL and GIA to the position of the present-day margin we choose the ICE-6G_C model as our base model as described above.

We note that ICE-6G_C does not account for ice mass changes associated with the LIA, during which the ice sheet slightly advanced to its historical maximum before receding to its current position. The maximum extent in ICE-6G_C, therefore, refers to both a pre-LIA extent that closely approached but did not yet reach the historical maximum (i.e. LIA) extent, as well as the post-LIA (i.e. present-day) extent. We use the LIA ice history from Adhikari et al. (2021) to account for the effects of ice mass changes during the LIA on modern sea level and VLM as a separate component (described in more detail in section 2.2.2). We note that this causes a slight inconsistency in one set of our models, those in which ICE-6G_C is modified to reach its modern maximum extent at the present day. In those scenarios, the effects of ice changes during the LIA are superimposed onto the effects of a linearly increasing (instead of stationary) ice mass between the ice margin minimum and the present day. Nonetheless, we consider this run instructive to understand the effects of the latest possible historical maximum extent on sea level change.

We employ a suite of Maxwell viscoelastic Earth structures to calculate the sea-level response. The density and elastic properties of the Earth models follow the 1D Preliminary Reference Earth Model (Dziewonski and Anderson, 1981). We employ three radially symmetric (1D) viscosity profiles (Table 1). The 1D profiles were obtained by fitting RSL observations around Greenland (Fleming and Lambeck, 2004; Lecavalier et al., 2014; Roy and Peltier, 2017). While some of these profiles were obtained when paired with different ice histories, we argue that they still provide a sensible range to explore the sensitivity of our results to mantle viscosity. Further, we run a smaller set of sensitivity tests only on the original and "no retreat" scenarios using a radially and laterally heterogeneous (3D) viscosity structure where 3D perturbations are imposed onto an average lithosphere thickness and upper and lower mantle viscosity (Table 1). The radial and lateral variations are derived from shear wave speed (see Austermann et al., 2021 for details; Richards et al., 2020) and are based on the tomography model by Schaeffer and Lebedev (2014).

In addition to predicting past sea level change, we also calculate the present-day rate of change over the last time step (0.25-0 ka), which we compare to observations that are described in section 2.2. Note that the rate of change does not vary appreciably over the last 250 years of the model. We further calculate the present-day vertical land motion rate.

Table 1: Earth viscosity profiles used to model the RSL response, with elastic thickness of the lithosphere (LT), upper mantle viscosity (UMV), and lower mantle viscosity (LMV). The boundary between the upper and lower mantle is at 670 km depth. Earth model E2 is VM5a (Roy and Peltier, 2017), which has separate viscosities for the upper and lower sections of the lower mantle. This

Pa s). Values for the 3D viscosity model correspond to the radial averages.

Model	LT (km)	UMV (10 ²¹ Pa s)	LMV (10 ²¹ Pa s)	1D/3D	Reference
E1	80	0.4	10	1D	(Fleming and Lambeck, 2004)
E2	60 (100)	0.5	1.57/3.23 (upper/lower)	1D	(Roy and Peltier, 2017)
E3	120	0.5	2	1D	(Lecavalier et al., 2014)
E4	96	0.5	5	3D	(Austermann et al., 2021)

2.2 Data constraints

2.2.1 Paleo sea-level data

We use three sea-level index points and two terrestrial upper-limiting points from the site 'Nuu', as described in Lecavalier et al., (2014). This site is closest to the location of the tide gauge and VLM records in Nuuk and will therefore be used as a paleo constraint to evaluate the modeled RSL responses for each combination of ice sheet history and Earth model. Further, we use the marine limit which constrains the highest point the RSL reached during deglaciated conditions. The sea-level records are derived from previous mapping efforts of the regional marine limit (Weidick, 1974) and radiocarbon-dated lake sediment packages from a site ~50 km northeast of Nuuk in Godthåbsfjord (Fredskild, 1983; Lecavalier et al., 2014) (Figure 1). Additional sea-level index points, terrestrial upper-limiting points, and lower-limiting points at Sisimiut, Sondre,

Godmouth, and Godhead, as summarized by Lecavalier et al., (2014), exist in the region and will be compared to the inferred RSL history in the discussion section 4.1.

2.2.2 Relative sea level budget and tide gauge data

We compare our GIA modeling results to the present-day RSL rate, derived from a 1958-2002 tide gauge record from Nuuk (64.17 N, 51.73 W; Figure 1), using the RSL budget framework laid out in Spada et al. (2014). By splitting the Nuuk tide gauge time series into empirically orthogonal intrinsic mode functions, which describe the variations in cyclicity, and removing the dominant components from the record including the 18.6-year nodal tide cycle, a standard linear regression on the residual results in an RSL rate of 1.93 ± 0.18 mm/yr.

We use the observed RSL rate to solve the RSL budget in Nuuk (Spada et al., 2014), which consists of several components:

$$260 s_{GIA} = s_{TG} - (s_{GIA_LIA} + s_{GrIS} + s_{AIS} + s_{GIC} + s_{TER} + s_{SDY}) (1)$$

where s_{GIA} is the rate of sea-level change driven by deglacial and Holocene ice sheet variability. In this section, we describe how we obtain a data-driven estimate of this quantity, which we will then compare to the model-driven estimate of this quantity as described in section 2.1. s_{TG} is the observed RSL rate from Spada et al. (2014), s_{GIA_LIA} is the rate of sea-level change driven by GIA effects related to recent ice mass changes (1000-2003 CE; related to the LIA), s_{GrIS} , s_{AIS} , and s_{GIC} are the sea-level changes driven by present-day ice mass changes associated with the GrIS, AIS, and other glaciers and ice caps, respectively, s_{TER} is the rate of sea-level change driven by changes

in terrestrial water mass exchange; and *sspy* is the rate of sea-level change rate driven by sterodynamic effects.

271

272

273

274

275

276

277

278

279

280

281

282

283

284

285

286

287

288

289

290

291

269

270

In the Nuuk/KNS region, the maximum historical extent was reached during the LIA in the 18th century (Lea et al., 2014; Pearce et al., 2022; Weidick et al., 2012). Adhikari et al. (2021) suggest that these relatively recent ice mass changes paired with low viscosities in the asthenosphere contribute to modern VLM, reconciling a longstanding mismatch between observed and modeled estimates of GNSS-derived VLM (Khan et al., 2016). Adhikari et al. (2021) justify a lower viscosity for these ice sheet changes that occurred more recently by invoking transient behavior in rheology (Paxman et al., 2023). We use the ice history from Adhikari et al. (2021) that extends from AD 1000 - 2003 and pair it with 120 Earth models that range in lithospheric thickness (60 -240 km) and mantle viscosities (isoviscous, $0.4 - 2.5 \cdot 10^{20}$ Pa s). These ranges in Earth parameters have been shown to produce fits to VLM Greenland-wide. Adhikari et al. (2021) show that the resulting VLM is not very sensitive to the mass anomaly prior to the little ice age and the timing of its onset (within the range tested). They do, however, show that data constrain the mass anomaly during the little ice age and the timing of retreat (AD 1865 ± 30). We use their preferred timing of maximum ice extent and retreat and ice mass anomalies. We use the GIA model described in section 2.1 to predict sea-level change and vertical land motion driven by this mass anomaly between 1965-2003. Note that no ice mass change is assumed during this time as the modern contribution of the GrIS is captured in s_{GrIS}. We calculate the model likelihood for each Earth structure based on fits to observed VLM from 57 GPS stations around Greenland from the Greenland Global Positioning System Network (GNET), a set of bedrock-based GNSS installations around Greenland (Bevis et al., 2012), following the approach by Adhikari et al.

(2021). Using the likelihood as model weights allows calculating a weighted mean and weighted standard deviation of the RSL rate ($s_{GIA\ LIA}$).

For the terms *sGrIS*, *sAIS*, and *sGIC*, we use sea-level fingerprints from Spada et al. (2014) to translate global mean (or ice equivalent) sea-level change to local sea-level change. Spada et al. (2014) determined sea-level fingerprints at the tide gauge location in Nuuk of -5.5, 1.1, and 0.25 for GrIS, AIS, and GIC melt, respectively, by solving the sea-level equation using SELEN (Spada and Stocchi, 2007). The authors calculate the sea-level fingerprints assuming uniform mass variation for the period 1961-2003 as reported by the Fourth Assessment Report of the Intergovernmental Panel on Climate Change (Solomon et al., 2007). Because more recent estimates of the global mean contributions of the GrIS, AIS, and GIC are not directly available over the exact period 1958-2002 (Fox-Kemper et al., 2021), we use the available estimates that cover the periods 1901-1990, 1971-2018, 1993-2018, and 1901-2018. For each estimate of the GrIS, AIS, and GIC and for each period, we calculate the weighted contribution based on the fraction of the 1958-2002 period that it covers and then determine the weighted mean for the GrIS, AIS, and GIC.

The global mean contribution together with the fingerprint allows calculation of the local RSL rate in Nuuk (Table 2). The contribution from terrestrial water storage (s_{TER}), assumed to be globally uniform with a rate of -0.07 ± 0.07 mm/yr and similar over the tide gauge period (1958-2002), is calculated from a combination of groundwater extraction and reservoir impoundment data over the period 1961-2003 (Slangen, 2012). Lastly, sterodynamic effects (s_{SDY}) can affect the RSL in Nuuk. These include steric effects, which refer to variations in sea level due to changes in ocean water density through temperature changes (thermosteric) and salinity changes (halosteric), as well

as dynamic effects, which refer to changes in ocean circulation in response to steric sea-level changes. The ocean dynamics response is particularly unconstrained in remote shallow coastal areas with limited observational data, such as the tide gauge location in Nuuk. To account for this uncertainty we calculate the variation from 23 ocean reanalyses (Dangendorf et al., 2021), which results in a 1 σ uncertainty of 2.19 mm/yr. Since the individual ocean reanalysis runs show limited skill in explaining the observed RSL in Nuuk, we do not include a mean sterodynamic contribution in our RSL budget.

We use the values described here (with uncertainties propagated) to obtain a data-driven estimate of s_{GIA} . We then compare this to the RSL rates predicted from the 35 s_{GIA} scenarios described in section 2.1.

Table 2: RSL rates in Nuuk for the period 1958-2002 for each contributor.

Contributor	Global SL rate	Fingerprint	Contribution to Nuuk RSL rate
	[mm/yr]	in Nuuk [-]	[mm/yr]
GrIS	0.33 ± 0.042	-5.5	-1.82 ± 0.23
AIS	0.088 ± 0.051	1.1	0.097 ± 0.056
GIC	0.54 ± 0.071	0.25	0.14 ± 0.018
TER			-0.07 ± 0.07
SDY			0 ± 2.19

2.2.3 GNSS data

We use data from the Greenland Global Positioning System Network (GNET), a set of bedrock-based GNSS installations around Greenland (Bevis et al., 2012). Khan et al. (2016) modeled the Earth's elastic response to present-day ice mass loss by assimilating a suite of remote sensing laser and radar altimetry data and removed it from the GNET GPS signal to isolate a VLM rate due to viscoelastic effects (GIA) of -1.3 ± 0.3 mm/yr for the period 2009-2016, co-located and partly contemporaneous with the tide gauge. Adhikari et al. (2021) performed a similar correction with an updated ice history for the period 2011-2017 and obtained a higher VLM rate due to GIA of -0.44 ± 0.48 mm/yr. These significant differences highlight the importance and uncertainty of the elastic correction. In our analysis, we choose to use both estimates to account for potential systematic biases in the elastic correction.

We use the observed and modeled viscous VLM rates to solve the VLM budget at Nuuk:

$$r_{GIA} = r_{GPS-elastic} - r_{GIA\ LIA} \tag{2}$$

The left-hand side (r_{GIA}) compares to the VLM rate predicted from the suite of runs described in section 2.1. $r_{GPS-elastic}$ is the GPS-derived VLM rate that has been corrected for the elastic effect of contemporaneous ice mass changes and r_{GIA_LIA} refers to the GIA effects of more recent ice mass changes on VLM during the LIA. r_{GIA_LIA} is calculated as described in section 2.2.2 (r_{GIA_LIA}) but by extracting VLM rather than sea level from the model prediction. We use the values described

here (with uncertainties propagated) to quantify the data-driven estimate of r_{GLA} and compare it to the VLM rates estimated from the 35 r_{GLA} scenarios described in section 2.1.

352

353

354

355

356

357

358

359

360

361

362

363

364

365

366

367

368

369

370

371

350

351

3. Results

3.1 Holocene relative sea-level curves

Holocene RSL changes at the paleo sea-level observation location near Nuuk exhibit considerable variability depending on the local ice history, lithosphere thickness, and upper and lower mantle viscosities (Figure 3). The retreat and readvance in the original ICE-6G C ice history leads to an RSL fall several meters below the modern RSL at Nuuk during the late Holocene and a subsequent RSL rise closer to the present day, forming the characteristic J-shape, which is visible for all Earth model parameters (Figure 3, yellow lines). The magnitude and timing of the drop, however, depend on the solid Earth properties. Simulations with a thick elastic lithosphere (120, E3; and 96 km, E4) lead to a low RSL at ~10 ka which is consistent with the marine limit. Conversely, simulations with a thinner elastic lithosphere (60/100km, E2; and 80km, E1) are not consistent with the marine limit at ~10 ka. Further, simulations with a thin lithosphere and low lower mantle viscosity (1.57/3.23 10²¹ Pa s; E2) lead to the highest sea-level low-stand during the mid-Holocene compared to simulations with the other Earth models. The Earth structures also vary in lower mantle viscosity, which may contribute to differences in RSL given the influence of the Laurentide ice sheet in this region. The fit to the sea-level index points is best for the 3D viscosity model E4, which shows the closest fit to all three points. The fit is slightly worse for models E1, E2, and E3. It should be noted that a perfect fit to all three index points within uncertainty is not likely given the general shape of our sea-level curves.

The adjusted ice history without retreat and readvance (Figure 3, red lines) shows a clear deviation from the original ice history with a less pronounced RSL drop (E3 and E4) or even a lack of negative RSL (E1 and E2).

376

377

378

379

373

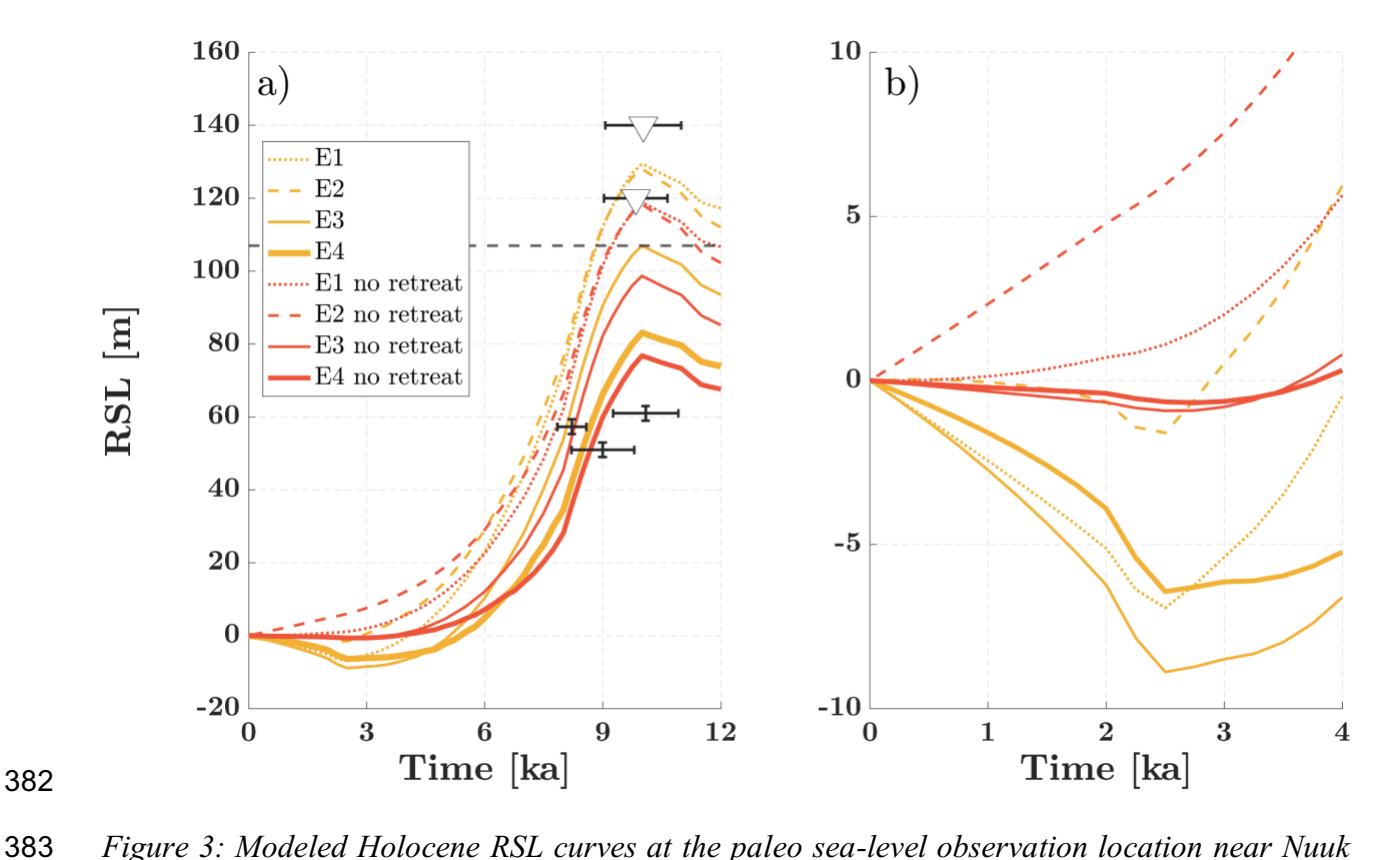
374

375

Omitting the retreat and readvance tends to lower the RSL curve during the early Holocene, slightly increasing the fit of the modeled RSL curves and the youngest sea-level index points for models E1 and E2. For E3 and E4, it is not clear whether omitting retreat improves the fit to the index points.

381

380



382

384

385

Figure 3: Modeled Holocene RSL curves at the paleo sea-level observation location near Nuuk (64.48° N, 50.997° W) for the original ICE-6G C (orange) and "no retreat" ICE-6G_C (red) ice histories, a) last 12 ka, b) last 4 ka. Both ice history variations are combined with four Earth models as described in Table 1. Paleo sea-level observations ($\pm 1\sigma$) are denoted by crosses (index

points) and downward triangles (terrestrial upper-limiting). The marine limit is denoted by the dashed grey line (Lecavalier et al., 2014). Note that the LIA ice variability is not included in the ICE-6G_C runs.

The timing of retreat and readvance shapes the Holocene RSL curves. A later retreat (minimum at 5, 4, and 3 ka) delays the ice mass unloading and leads to higher RSL during the early and mid-Holocene and lower RSL in the late Holocene, and thus a more pronounced RSL drop below 0 m (Figure 4). Similar to the original ice histories (Figure 3), the choice of Earth model results in different magnitudes and timings of the RSL maxima and minima. Delaying the readvance to 1 ka or the present causes a later sea-level reversal and consequently (since RSL curves are sea level relative to the present) an overall higher RSL curve with a later, shallower sea-level dip. Simulations with Earth model E3 provide the best fit to the sea-level index points and most runs remain below the marine limit (Figure 4c), while the early-Holocene RSL for simulations with Earth models E1 and E2 are not consistent with the marine limit. For all Earth models, the data-model fit is slightly higher if the ice sheet approaches its maximum at 1 or 2 ka.

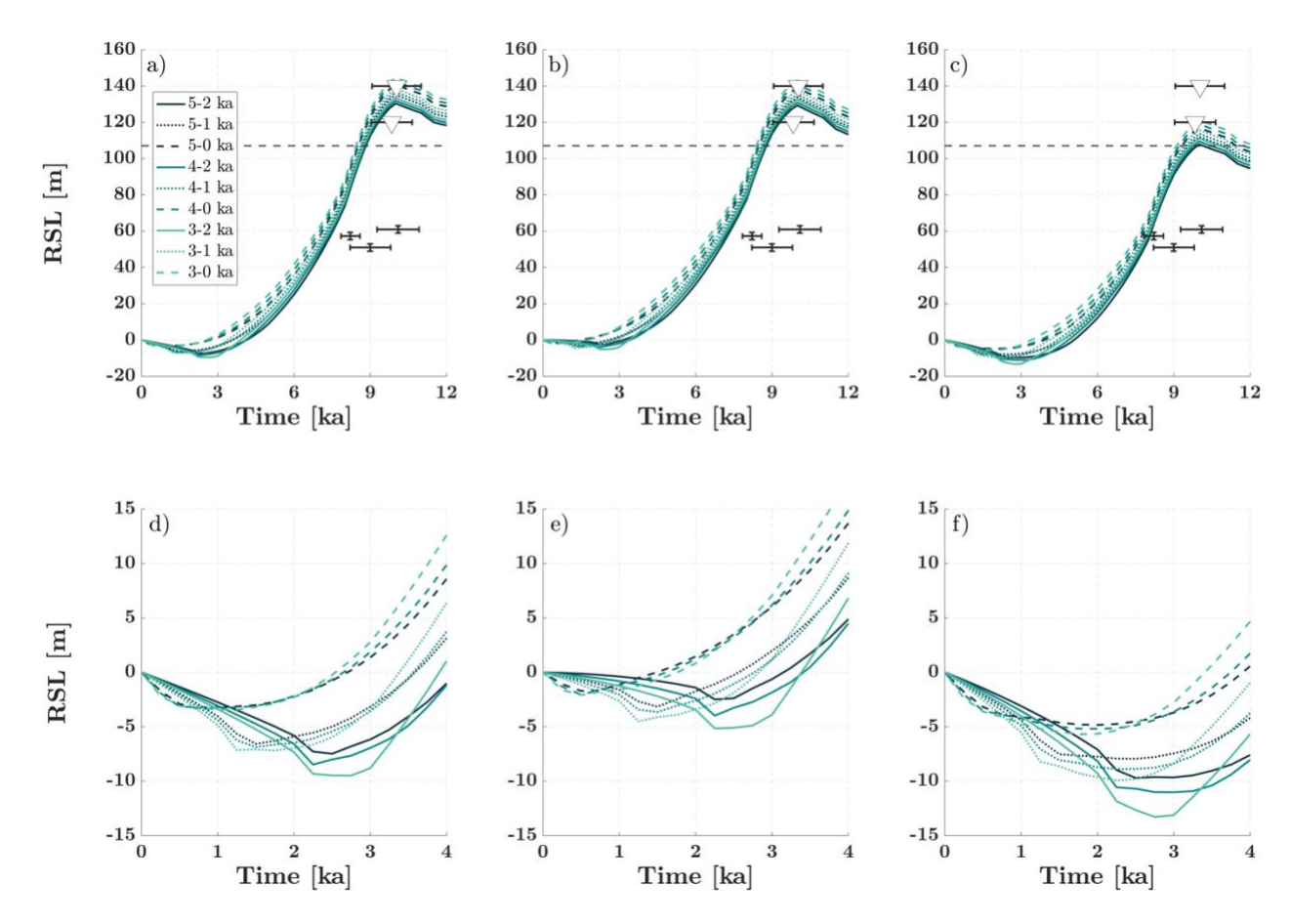


Figure 4: Modeled Holocene RSL curves at the paleo sea-level observation location near Nuuk $(64.48^{\circ} \text{ N}, 50.997^{\circ} \text{ W})$ for the ICE-6G_C ice histories with adjusted timing of ice the sheet minimum and adjusted timing of when the ice sheet reaches its current maximum extent (legend shows the periods from the minimum to the maximum extents), combined with Earth model: a) E1, b) E2, and c) E3. Plots d, e, and f show the same sea-level curves as plots a, b, and c, but zoomed in on the last 4 ka. Paleo sea-level observations (\pm 1 σ) are denoted by crosses (index points) and downward triangles (terrestrial upper-limiting). The marine limit is denoted by the dashed grey line (Lecavalier et al., 2014). Note that the LIA ice variability is not included in the ICE-6G_C runs.

Overall, the original and "no retreat" ice histories, as well as the ice histories with adjusted timings paired with Earth model E3 produce RSL curves that are most consistent with the paleo sea-level observations. Most of these ice scenario-Earth model combinations cross or closely approach at least one index point (most often the youngest index point). The 3D Earth model (E4) RSL curves without retreat have the highest data-model fits by closely approaching all three index points, showing that the 3D variations in the solid Earth parameters improve the fit of the modeled RSL to the sea-level observations.

3.2 Present-day relative sea-level rates

The modeled present-day RSL rate at Nuuk is contingent on the choice of ice history and solid Earth properties. We test the modeled RSL rates by comparing them with the observationally inferred deglacial GIA rate (r.h.s of Equation 1; 4.92 ± 2.24 mm/yr), which consists of correcting the tide gauge inferred sea-level rate for several components detailed in section 2.2 (Figure 5). One of the components that we model separately is the RSL rate due to ice mass changes during the LIA (s_{GIA_LIA}). We find that this causes a present-day rate of sea-level change of -1.34 \pm 0.34 mm/yr. An RSL fall for this component is expected since the ice mass unloading of the late-LIA retreat results in present-day solid Earth uplift and decreased gravitational attraction of ocean water.

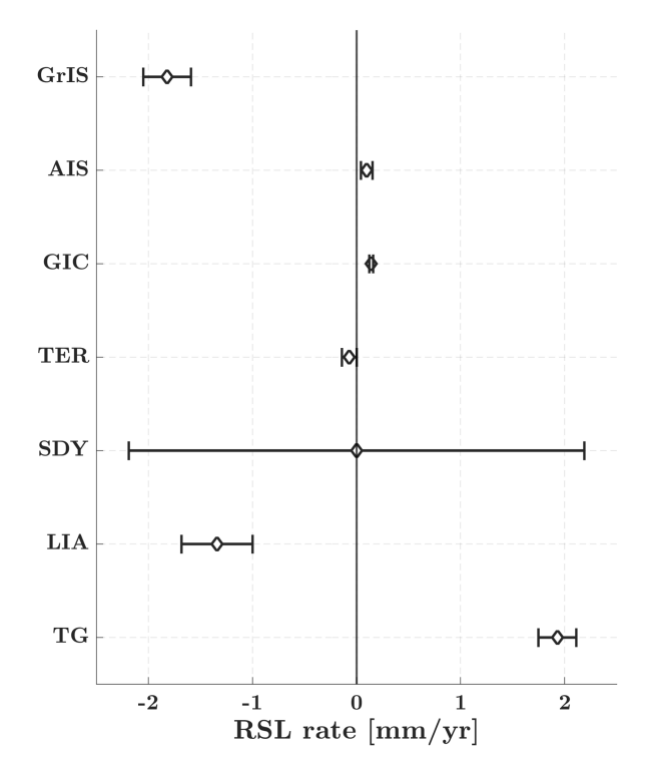


Figure 5: Individual contributions of each component to s_{GIA} (right-hand-side of Equation 1, Table 2) in Nuuk for the period 1958-2002.

The RSL rates driven by the original ICE-6G_C ice history predict sea-level rise, which is driven by the GIA effects associated with ice readvance. However, the rates underestimate the observationally constrained target value, with models E1 and E3 producing a closer fit to the observations than E2 and E4 (Figure 6, empty orange squares). The RSL rates using the "no retreat" ice history are lower than those with retreat because their RSL curve lacks a "dip" (Figure 3). As a result, these data fit the observational constraints worse than the original ice history, indicating that some inland retreat of the ice margin is necessary. The ice histories where the ice sheet minimum is shifted to 5, 4, and 3 ka, perform similarly to the original ICE-6G_C ice history (Figure 6, small squares) with slightly higher rates for a later minimum. This indicates that the RSL rate is only slightly sensitive to the timing of the ice sheet minimum within the range 6-3 ka.

Forcing the ice sheet to approach the historical maximum closer to the present day, instead of at 2 ka, significantly increases the RSL rate and the data-model fit. For model E1, model runs that approach the historical maximum at 1 ka or the present (with a minimum achieved sometime between 5-3 ka) lead to RSL rates that fall within the uncertainty of the observationally constrained rate (Figure 6, light grey band). It should be noted that, as described in section 2.1, the scenario in which the ice margin does not approach the historical maximum extent until present-day is not strictly consistent with geological constraints. Nonetheless, we show this scenario here to understand the effect of a slower rate of Holocene ice mass growth on the present-day sea level rate. For model E2, only runs that reach the maximum extent at present-day are able to fit the data constraints within uncertainty (i.e. fall within the light grey region in Figure 6). In the case of model E3, most simulations with a delayed minimum at or after 5 ka, and an approach to the historical maximum at or after 2 ka, fall within the data uncertainty. Neglecting uncertainties associated with the sterodynamic component would significantly decrease the target range (Figure 6, dark grey band) and reduce the number of model runs consistent with the observationally constrained estimates only allowing models with a later (1 ka to present) readvance.

462

463

464

465

466

467

468

447

448

449

450

451

452

453

454

455

456

457

458

459

460

461

In addition to changes in the timing, it has been suggested that the magnitude of retreat and readvance in ICE-6G_C is overestimated by a factor of 3-4 (Lesnek et al., 2020; Young et al., 2021). A retreat of smaller magnitude is expected to cause an RSL dip of lower magnitude, similar to the effect of the "no retreat" scenario, and would therefore produce a lower RSL rate in each scenario. That means it would likely limit the range of models that fall within the observational constraints to those that readvance close to present-day.

We tested the impact of the LIS on the present-day RSL rate in Nuuk (Figure 6, filled orange squares) by substituting the LIS in ICE-6G_C with the LIS from the ice sheet model GLAC1-D (Tarasov et al., 2012). The resulting RSL rates are slightly higher, showing some sensitivity to the LIS, but do not significantly affect the results.



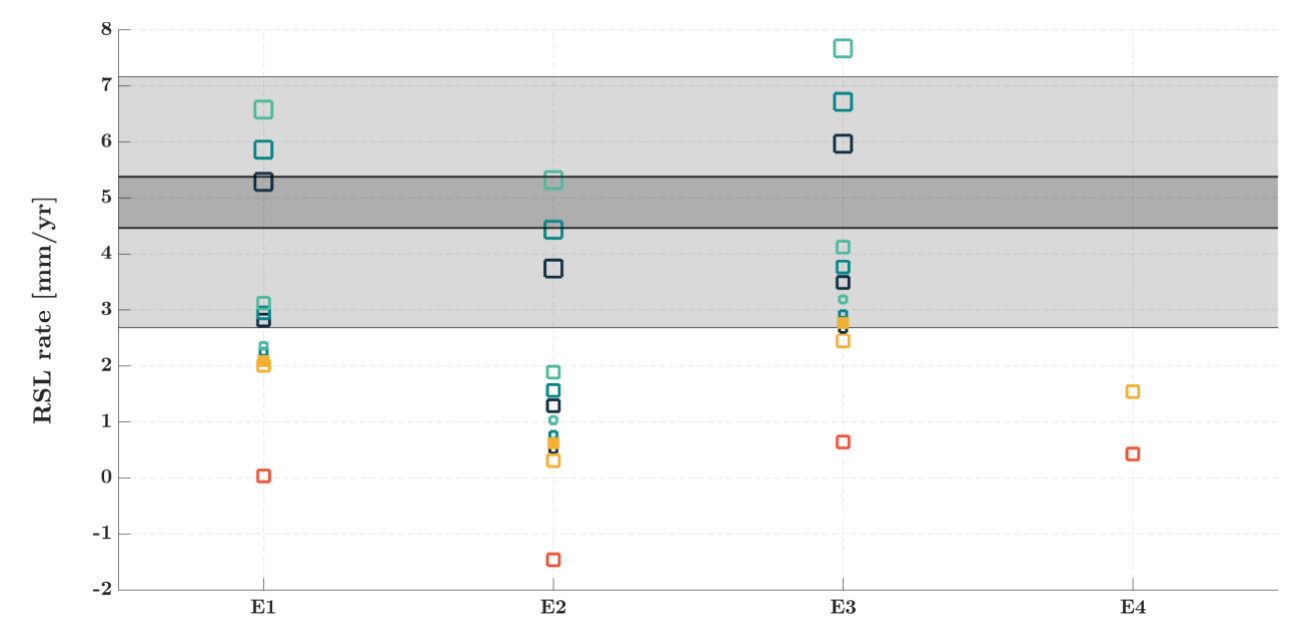


Figure 6: Comparison of modeled present-day RSL rates in Nuuk (64.17° N, 51.73° W) driven by deglacial GIA for every ICE-6G_C ice history: original (empty orange); no retreat (red); and ice sheet minimum at 5 ka (dark green), 4 ka (green), and 3 ka (light green). The size of the dark/normal/light green markers indicates the timing when the ice sheet reaches its current maximum extent at: 2 ka (small), 1 ka (medium), and present-day (large). Filled orange squares show modeled RSL rates where the LIS in ICE-6G_C was substituted with the LIS in GLAC1-D (Tarasov et al., 2012). The observationally estimated RSL rate driven by deglacial GIA (as detailed in section 2.2, Equation 1) is denoted by the light grey shaded area (± 1 σ range). The dark grey area indicates a more restricted uncertainty that excludes the uncertainty in sterodynamic effects.

3.3 Present-day vertical land motion rates

We evaluate the modeled VLM rates through comparison with the observationally inferred deglacial VLM rate (r.h.s of Equation 2) which yields a value of -2.88 ± 0.48 mm/yr when using $r_{GPS-elastic}$ from Khan et al. (2016) and -2.02 ± 0.58 mm/yr with $r_{GPS-elastic}$ from Adhikari et al. (2021). We find the modeled VLM rate due to ice mass changes during the LIA (r_{GIA_LIA}) to be 1.58 ± 0.38 mm/yr. As expected, ice mass loss since the LIA leads to rebound.

492

493

494

495

496

497

498

499

500

501

502

503

504

505

506

507

486

487

488

489

490

491

The VLM rates using the original ICE-6G C ice history, paired with models E1, E3, and E4 fall within the observationally derived VLM rate (Figure 7) when using *r_{GPS-elastic}* of Khan et al. (2016). The original ice history paired with E2 overestimates the observationally derived VLM rates for both estimates of r_{GPS-elastic}. For all Earth models, predictions for the "no retreat" ice history overestimate the observationally derived VLM rates. For E1, E2, and E3, a later timing of the minimum extent (closer to 3 ka) lowers the modeled VLM rates. For E1 and E3, the modeled VLM rates remain within the uncertainty of the observationally derived VLM rates. For E2, a later timing of the minimum extent brings the prediction closer to the observed VLM rates. However, for E1, E2, and E3, the sensitivity to the timing of the minimum extent is again relatively small. Forcing the historical maximum to be approached at 1 ka and present-day lowers the modeled VLM rates more significantly. For E1, the modeled VLM rates remain within the uncertainty of the observationally derived VLM rate using r_{GPS-elastic} from Adhikari et al. (2021) when the maximum extent is approached at 1 ka, but underestimates the observed VLM rates when the maximum is reached at present-day. For E2, forcing the maximum extent to be approached at 1 ka increases the fit to the observationally derived VLM rates, where a late minimum extent (3 ka) provides the best fit. For E3, the modeled VLM rates underestimate the observationally derived VLM rates when the maximum extent is reached at 1 ka or present-day.

A smaller magnitude of retreat and readvance (than in ICE-6G_C) as suggested by Lesnek et al. (2020) and Young et al. (2021) is expected to cause a less pronounced present-day solid Earth deformation, similar to the effect of the "no retreat" scenario. The modeled VLM rates would, therefore, be less negative and, for E1 and E3 would improve the fit to the observationally derived VLM rate, while for E2 and E4, this would reduce the data-model fit. This would likely limit the range of models that fall within the observational constraints.

Similar to the RSL rate analysis, we tested the impact of the LIS on the present-day VLM rate. Substitution with the LIS from GLAC1-D results in slightly lower VLM rates, but the results are not significantly affected.

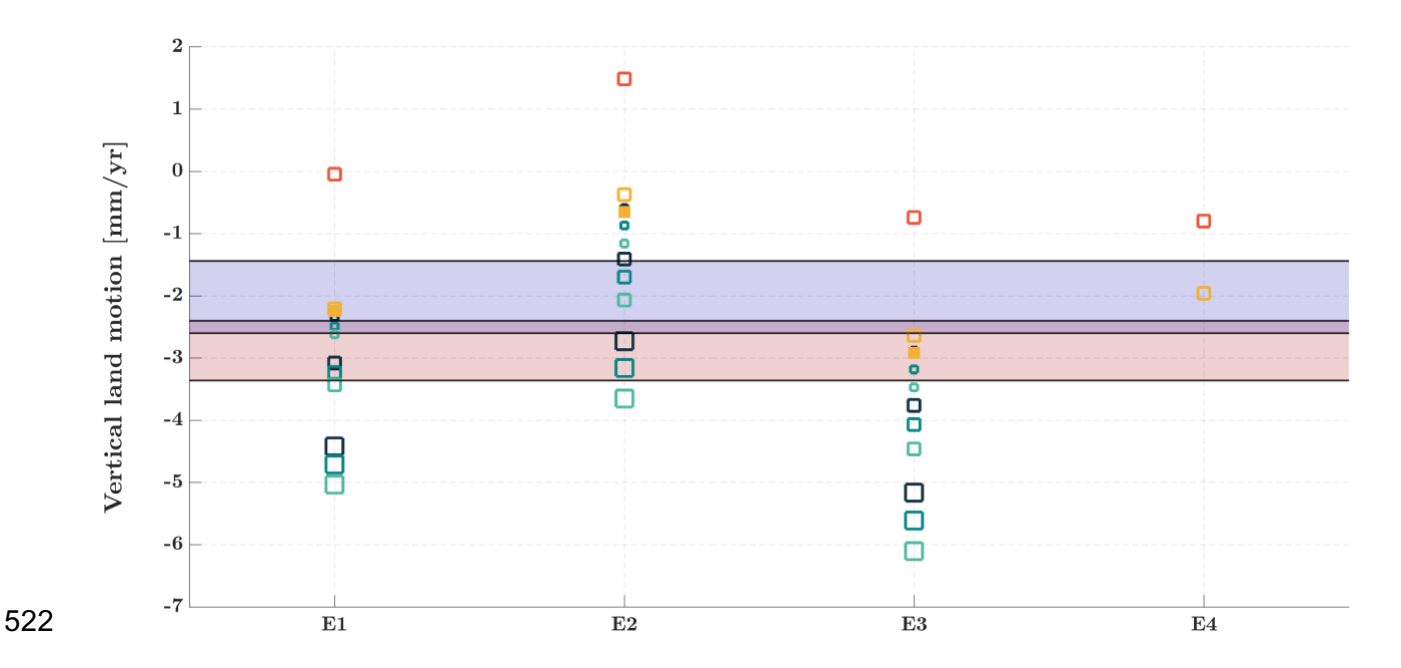


Figure 7: Comparison of negative modeled present-day VLM rates in Nuuk (64.17° N, 51.73° W) for every ICE-6G_C ice history: original (orange); no retreat (red); and ice sheet minimum at 5 ka (dark green), 4 ka (green), and 3 ka (light green). The size of the dark/normal/light green markers indicates the timing when the ice sheet reaches its current maximum extent at: 2 ka (small), 1 ka (medium), and present-day (large). Filled orange squares show modeled RSL rates where the LIS in ICE-6G_C was substituted with the LIS in GLAC1-D. The observationally inferred deglacial VLM rate (Equation 2) is denoted by the blue and red shaded areas (± 1σ range), with r_{GPS-elastic} from Khan et al. (2016) and Adhikari et al. (2021), respectively. The purple shaded area denotes where the two estimates overlap. The Earth model used is indicated at the bottom.

4. Discussion

4.1 Constraints on ice retreat and readvance in SW Greenland

Our results suggest that some degree of inland ice sheet retreat in southwestern Greenland near Nuuk is necessary during the mid/late-Holocene to fit the model output to the data. The RSL and VLM rates using Earth model E1 simultaneously satisfy the observational constraints if the historical maximum extent is approached at 1 ka without a strong constraint on the timing of retreat. Note, however, that the RSL predictions are at the edge of the data-derived uncertainty range, while the VLM predictions are well within the observational constraints. For model E2, the RSL and VLM predictions only satisfy both data-derived constraints simultaneously if the maximum extent is reached at present-day, which is an unlikely end-member since this setup is not consistent with geological constraints. This Earth model therefore seems the least appropriate for this region. The RSL and VLM rates using model E3 satisfy the observational constraints if the historical maximum is reached at 2 ka and the minimum occurred at 5 ka or later. Note that the

RSL predictions are again at the edge of the data-derived uncertainty range. However, simulations with Earth model E3 satisfy the early-Holocene marine limit and closely approach the sea-level index points. For model E4, the RSL and VLM predictions for the original ICE-6G_C and the "no retreat" ice histories are not consistent with the observational constraints, suggesting that this Earth model would also require a delayed timing of the minimum and maximum extents. Based on these results we argue that the minimum extent of the southwest GrIS near Nuuk was likely reached at or after 5 ka, and perhaps as late as 3 ka. Additionally, we conclude that the historical maximum extent of the southwest GrIS was likely approached between 2 and 1 ka.

To further test these inferences, we simulated the RSL history at four additional locations in southwest Greenland (Figure 1). Earth model E2 produces a reasonable fit in Sisimiut (Figure 8a) but systematically shows a poor alignment with the remaining paleo sea level data (Figures 8 c, e, and g), which agrees with the results discussed above. The preferred model setup (model E3, minimum at 5 ka or after, maximum between 2 and 1 ka) does not show a good fit in Sisimiut (Figure 8b) but generally satisfies the sea level constraints at the other locations except for overpredicting sea level in the early Holocene (Figures 8 d, f, and h). This further supports our preference for this ice history and Earth model configuration.

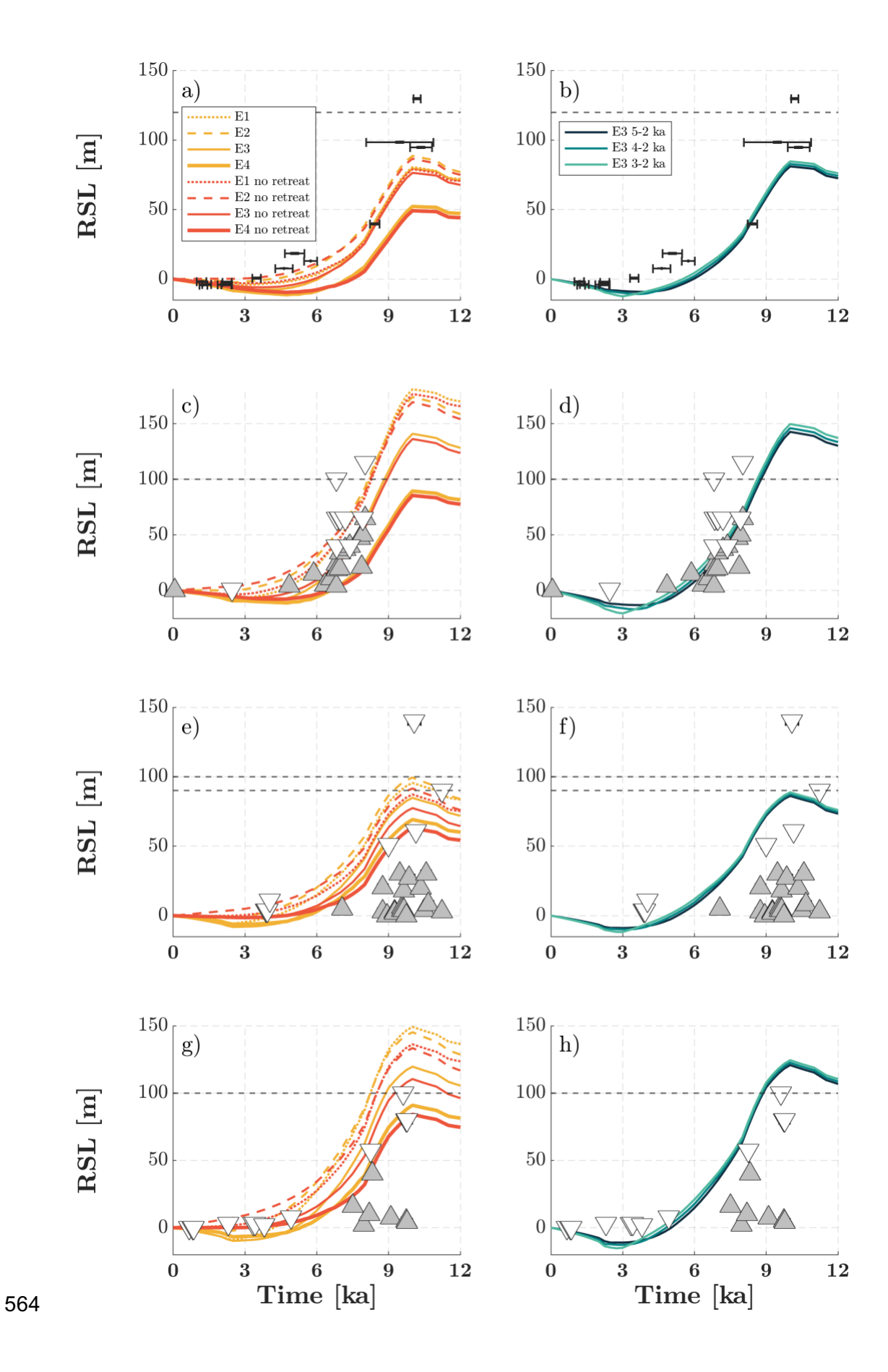


Figure 8: Modeled Holocene RSL curves for the original ICE-6G_C (orange) and "no retreat" ICE-6G_C (red) ice histories at a) Sisimiut, c) Sondre, e) Godmouth, and g) Godhead. Both ice history variations are combined with four Earth models as described in Table 1. Modeled Holocene RSL curves, paired with Earth model E3, with adjusted timing of the minimum ice extent (5, 4, and 3 ka) at b) Sisimiut, d) Sondre, f) Godmouth, and h) Godhead. The maximum ice extent is reached at 2 ka for all three runs. Paleo sea-level observations (\pm 1 σ) are denoted by crosses (index points), downward triangles (terrestrial upper-limiting), and upward triangles (marine lower-limiting). The marine limit is denoted by the dashed grey line (Lecavalier et al., 2014). Note that the LIA ice variability is not included in the ICE-6G_C runs.

The likely-overestimated ~130-140 km of retreat in ICE-6G_C can affect our modeled sea level responses - a smaller retreat magnitude than in ICE-6G_C would likely cause a less pronounced present-day solid Earth deformation, i.e. a less negative VLM and a less positive RSL rate, similar to the effect of the "no retreat" scenario. This would delay the likely timing of the approach to the historical maximum closer to the present day. We are not aware of an ice sheet model that broadly fits sea level constraints, correctly simulates the present-day ice extent, and only simulates ~10 km of ice retreat at the Holocene ice minimum. An ad-hoc combination of ice sheet models will likely create edge/interpolation effects that could affect our results in a physically-inconsistent way. We therefore opt to only incorporate ICE-6G_C into our model setup and acknowledge the impact of the larger retreat.

Our results are consistent with the results from Young et al. (2021), who estimate that the southwest GrIS minimum extent was likely reached after ~5 ka and that the late Holocene

maximum extent was reached during historical times despite the GrIS perhaps approaching (but not quite reaching) this eventual maximum as early as ~2 ka.

4.2 Sensitivity tests and model uncertainties

Adhikari et al. (2021) suggest that a transient rheology is necessary to fit VLM observations around Greenland. Paxman et al. (2023) combine shear wave velocities with experimentally constrained constitutive rheological models and also find that mechanical properties including the apparent upper mantle viscosity and lithosphere thickness vary over time. While we assume a Maxwell rheology in our GIA model setup that does not allow transient rheology, we do adopt a change in viscosity of about one order of magnitude in our corrections for the LIA period. Modeled sea level predictions are most sensitive to the inclusions of transient mantle deformation in regions nearfield and peripheral to former ice sheets (Simon et al., 2022), such as our study site near Nuuk. While we acknowledge the value in investigating the effect of transient rheology in our model setup, this aspect remains outside of the scope of this study. The choice of rheology as well as the importance of transient deformation remain to be further explored and a more complex rheology may affect our results.

The magnitude and timing of the disappearance of the LIS affects the modeled RSL in Nuuk. Southwest Greenland resides on the forebulge of the LIS, which has been subsiding since the melting of the LIS after the LGM. A larger LIS volume during the LGM, and thus a larger forebulge, may lead to a larger present-day subsidence rate and thus a larger RSL rate in Nuuk. Vice versa, a smaller LIS volume may result in a smaller RSL rate. Additionally, the timing of the LIS melting may affect the RSL rate in Nuuk by forcing the present-day subsidence rate to be

higher (lower) for a later (early) melting event. Nevertheless, we show that this effect is small: substituting the LIS in ICE-6G_C with the LIS from GLAC1-D results in a minor change in our modeled present-day RSL and VLM rates (Figures 6 and 7).

Sterodynamics play an important role in controlling RSL in southwest Greenland (Dangendorf et al., 2021). Both steric and ocean dynamic effects show complex patterns in shallow and remote coastal areas, such as our study location near Nuuk, that are currently understudied due to limited observational data. While we account for potential sterodynamic effects by including a relatively large sterodynamic uncertainty in our RSL budget, derived from ocean reanalyses (Dangendorf et al., 2021), we do not include a mean sterodynamic contribution in our RSL budget since the individual ocean reanalysis runs show limited skill in explaining the observed RSL in Nuuk. Properly incorporating sterodynamics into our analysis requires further work and analyses of the physical processes controlling sterics and ocean dynamics near Nuuk.

4.3 Relationship between ice sheet change and regional climate

Geologic reconstructions of ice-margin change and our modeling results presented here suggest that the southwestern GrIS may not have achieved its Holocene minimum extent until sometime after 5 ka, perhaps as late as 3 ka. The timing of this ice minimum is significantly later than what might be predicted by various hemispheric to regional forcing mechanisms (Figure 9). For example, high-latitude northern insolation peaked at ~11 ka (Berger and Loutre, 1991), whereas temperature reconstructions generally depict maximum Holocene temperatures around 8 ka at the GrIS summit (Kobashi et al., 2017). Moreover, simulations of GrIS change suggest mass loss was highest between ~11-8 ka (Buizert et al., 2018), broadly consistent with the timing of peak

insolation and maximum reconstructed temperatures from Summit Greenland. Yet, focusing in on select records more proximal to southwestern Greenland reveals perhaps a different relationship between ice-sheet behavior and temperature.

637

638

639

640

641

642

643

644

645

646

647

648

649

650

651

652

653

654

655

656

634

635

636

Badgeley et al., (2020) used a novel data assimilation approach to develop, arguably, the most robust temperature reconstruction across the southwestern Greenland domain (Figure 9). Interestingly, this reconstruction depicts rapidly warming temperatures between ~12-8 ka, peak Holocene temperatures between ~6-5 ka followed by a 1-2 kyr-long plateau, and no significant cooling until after ~4 ka (Badgeley et al., 2020; Briner et al., 2020). In the Sisimiut-Kangerlussuag region, the rate of ice-sheet retreat was highest between $\sim 10.4 - 9.1$ ka (Lesnek et al., 2020) and a recent ensemble of geologically benchmarked simulations of ice-sheet change in southwestern Greenland depict maximum rates of mass loss between ~12-7 ka followed by a relatively inbalance ice sheet for the remainder of the Holocene until modern times (Briner et al., 2020). Collectively, these records suggest that the rate of mass loss in southwestern Greenland was highest in the early Holocene as the ice sheet was significantly out of balance with rapidly warming temperatures and peak insolation. Through the middle Holocene, however, ice sheet mass balance stabilized and was largely in equilibrium with regional climate as 1) the rate of climate warming stabilized even if peak temperatures were slightly warmer (Badgeley et al., 2020; Figure 9), and 2) increased precipitation likely counteracted the effects of increased temperatures to some degree (i.e., Briner et al., 2020; Downs et al., 2020). At face value, our ice-sheet minimum with the best data-model fit in this study – after 5 ka, perhaps as late as 3 ka – is entirely consistent with the reconstructed surface mass balance in southwestern Greenland. That is, the majority of significant southwestern GrIS change had already occurred in the early Holocene, and slightly elevated

temperatures between ~6-5 ka and increased precipitation would result in relatively minor net retreat of the southwestern GrIS margin during the middle Holocene. The onset of significant cooling at ~4 ka likely marked the approximate transition between the ice sheet minimum and the regrowth towards the pre-industrial maximum ice extent, consistent with our modeling effort here.

On paleo and historical timescales, southwestern Greenland is dominated by surface mass balance with both temperature and precipitation strongly affecting ice-margin evolution (Mouginot et al., 2019; Cuzzone et al., 2019; Downs et al., 2020). Although, in the Nuuk region, ice dynamics likely influence ice-margin migration on millennial timescales (Cuzzone et al., 2022). Nonetheless, our results are consistent with the reconstructed evolution of ice sheet margin migration and mass balance in southwestern Greenland (i.e., Briner et al., 2020; Young et al., 2021), while at the same time highlighting the complicated balance between temperature, precipitation, and broad-scale ice sheet behavior through the Holocene.

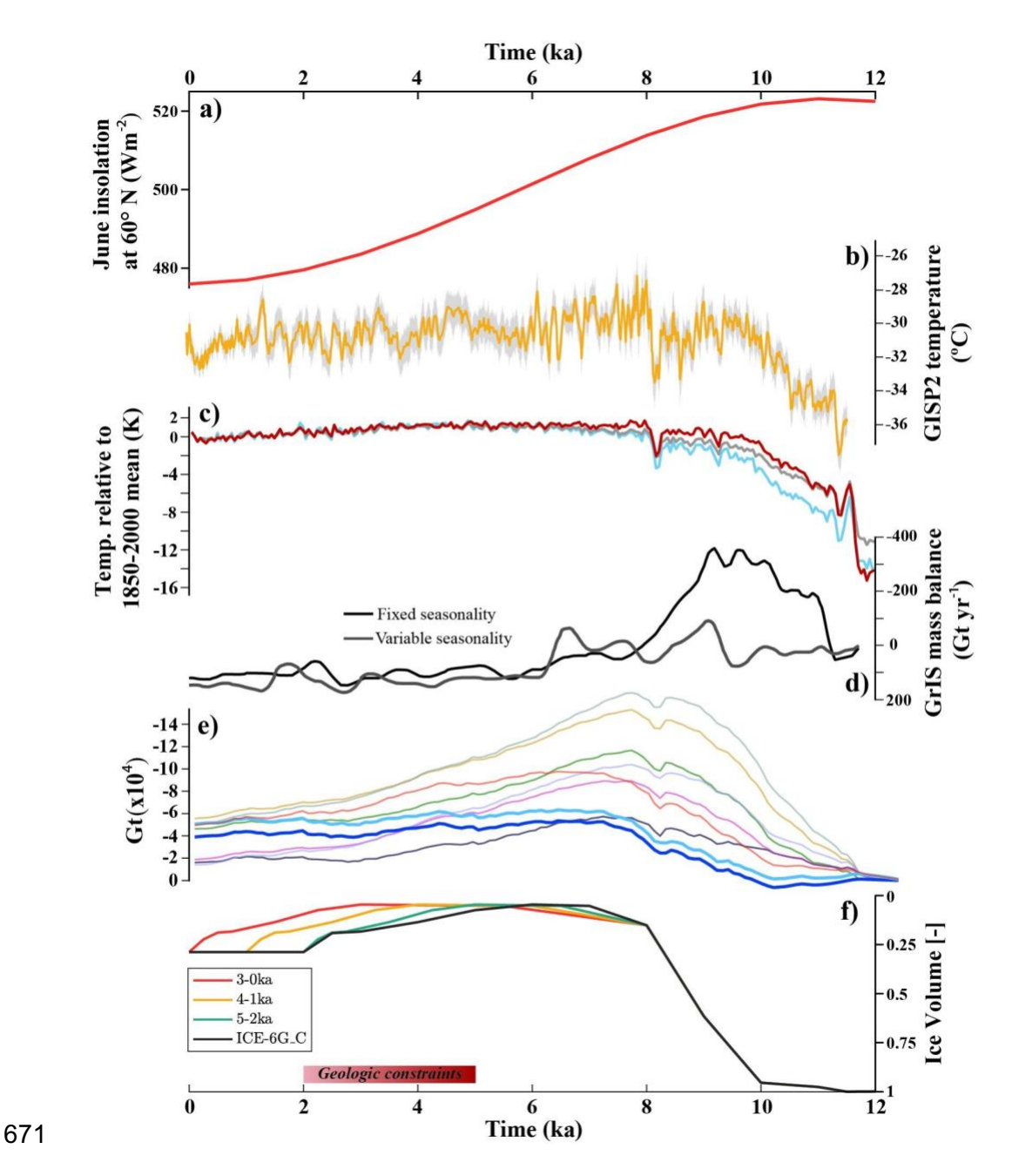


Figure 9: a) June insolation at 60° N (Berger and Loutre, 1991). b) Mean annual temperatures at the Greenland Ice Sheet Project 2 (GISP2) site reconstructed using gas-phase $\delta Ar-N_2$ measurements ($\pm 2\sigma$; Kobashi et al., 2017). c) Temperature anomalies over southwestern Greenland (Badgeley et al., 2020; Briner et al., 2020). d) Simulated GrIS mass balance forced by fixed (black line) and variable (gray line) temperature seasonality (Buizert et al., 2018). e) Nine simulations of ice mass in southwest Greenland through the Holocene using various climate

reconstructions (Briner et al., 2020; Young et al., 2021). In bold (blue) are the two simulations most consistent with the geologic record of ice-sheet change in southwestern Greenland (Young et al., 2021). f) Modeled southwest Greenland ice volume fraction from this study, similar to Figure 2. Note the inverted y-axis in panels d), e), and f). Geologic constraints suggest that the southwestern GrIS achieved its Holocene minimum sometime between 5-2 ka (Young et al., 2021).

683

684

685

686

687

688

689

690

691

692

693

694

695

696

697

698

699

700

682

678

679

680

681

5. Conclusions

Through our modeling approach, we explored a suite of scenarios of southwest GrIS retreat and readvance during the Holocene and the associated impacts on past RSL and present-day RSL and VLM changes near Nuuk. Our findings highlight the sensitivity of the Holocene and modern RSL and VLM to ice sheet history and Earth structure. Models that incorporate a retreat of the ice margin to the Holocene minimum extent between 5 and 3 ka and approach the historic maximum extent between 2 and 1 ka align most closely with our observational constraints. This provides valuable insight on the behavior of the GrIS to warmer temperatures. These constraints suggest that the timing of the southwest GrIS minimum reconstructed here is consistent with the likely evolution of southwestern GrIS mass balance through the Holocene. The GrIS is already responding to current warming and our results indicate that ice retreat will almost certainly continue as regional temperatures continue to increase. Yet, the exact response time of the southwestern GrIS to climate variability is difficult to establish given the century-to-millennial timescales of temperature maximum and ice sheet minimum events. Moreover, the inherent uncertainties of the observational data used in this study limit the strictness of the ice sheet behavior constraints. Nonetheless, the constraints highlighted in this study have implications for future ice sheet modeling of southwestern Greenland and provide a broader understanding of the

701	interactions between the climate and the cryosphere and, ultimately, of future ice sheet change.
702	Major areas for future work include improving the constraints on Earth structure and rheology
703	around Greenland and improving the sterodynamic contribution to RSL along the Greenland coast.
704	Further studies on the response of the GrIS to a changing climate are essential for understanding
705	ice sheet behavior and for refining sea level rise predictions and the consequences to coastal
706	regions around the world.
707	
708	Author contributions
709	Raf Antwerpen: Conceptualization, Methodology, Investigation, Data Curation, Formal Analysis,
710	Writing - Original Draft. Jacky Austermann: Conceptualization, Methodology, Supervision,
711	Writing - Review & Editing, Funding Acquisition. Nicolas Young: Supervision, Writing - Review
712	& Editing, Funding Acquisition. David Porter: Writing - Review & Editing. Lauren Lewright:
713	Data Curation, Writing - Review & Editing. Konstantin Latychev: Data Curation.
714	
715	Acknowledgments
716	We would like to thank Sönke Dangendorf for contributing to the ocean dynamics discussion. This
717	research was supported by the U.S. National Science Foundation: ICER 19-28146 (RA, JA, and
718	DP) and NSF-ARCSS #1503959 (NY).
719	
720	References
721	Adhikari, S., Milne, G.A., Caron, L., Khan, S.A., Kjeldsen, K.K., Nilsson, J., Larour, E., Ivins,
722	E.R., 2021. Decadal to Centennial Timescale Mantle Viscosity Inferred From Modern
723	Crustal Uplift Rates in Greenland. Geophys. Res. Lett. 48.

- 724 https://doi.org/10.1029/2021GL094040
- 725 Argus, D.F., Peltier, W.R., Drummond, R., Moore, A.W., 2014. The Antarctica component of
- postglacial rebound model ICE-6G_C (VM5a) based on GPS positioning, exposure age
- dating of ice thicknesses, and relative sea level histories. Geophys. J. Int. 198, 537–563.
- 728 https://doi.org/10.1093/gji/ggu140
- Austermann, J., Hoggard, M.J., Latychev, K., Richards, F.D., Mitrovica, J.X., 2021. The effect of
- lateral variations in Earth structure on Last Interglacial sea level. Geophys. J. Int. 227,
- 731 1938–1960. https://doi.org/10.1093/gji/ggab289
- 732 Badgeley, J.A., Steig, E.J., Hakim, G.J., Fudge, T.J., 2020. Greenland temperature and
- precipitation over the last 20 000 years using data assimilation. Clim. Past 16, 1325–1346.
- 734 https://doi.org/10.5194/cp-16-1325-2020
- 735 Berger, A., Loutre, M.F., 1991. Insolation values for the climate of the last 10 million years. Quat.
- 736 Sci. Rev. 10, 297–317. https://doi.org/10.1016/0277-3791(91)90033-Q
- 737 Bevis, M., Wahr, J., Khan, S.A., Madsen, F.B., Brown, A., Willis, M., Kendrick, E., Knudsen, P.,
- Box, J.E., van Dam, T., Caccamise, D.J., Johns, B., Nylen, T., Abbott, R., White, S., Miner,
- J., Forsberg, R., Zhou, H., Wang, J., Wilson, T., Bromwich, D., Francis, O., 2012. Bedrock
- displacements in Greenland manifest ice mass variations, climate cycles and climate
- 741 change. Proc. Natl. Acad. Sci. 109, 11944–11948.
- 742 https://doi.org/10.1073/pnas.1204664109
- 743 Briner, J.P., Cuzzone, J.K., Badgeley, J.A., Young, N.E., Steig, E.J., Morlighem, M., Schlegel, N.-
- J., Hakim, G.J., Schaefer, J.M., Johnson, J.V., Lesnek, A.J., Thomas, E.K., Allan, E.,
- Bennike, O., Cluett, A.A., Csatho, B., de Vernal, A., Downs, J., Larour, E., Nowicki, S.,
- 746 2020. Rate of mass loss from the Greenland Ice Sheet will exceed Holocene values this

- 747 century. Nature 586, 70–74. https://doi.org/10.1038/s41586-020-2742-6
- 748 Briner, J.P., McKay, N.P., Axford, Y., Bennike, O., Bradley, R.S., De Vernal, A., Fisher, D.,
- Francus, P., Fréchette, B., Gajewski, K., Jennings, A., Kaufman, D.S., Miller, G., Rouston,
- 750 C., Wagner, B., 2016. Holocene climate change in Arctic Canada and Greenland. Quat.
- 751 Sci. Rev. 147, 340–364. https://doi.org/10.1016/j.quascirev.2016.02.010
- 752 Briner, J.P., Stewart, H.A.M., Young, N.E., Philipps, W., Losee, S., 2010. Using proglacial-
- threshold lakes to constrain fluctuations of the Jakobshavn Isbræ ice margin, western
- Greenland, during the Holocene. Quat. Sci. Rev. 29, 3861–3874.
- 755 https://doi.org/10.1016/j.quascirev.2010.09.005
- Buizert, C., Keisling, B.A., Box, J.E., He, F., Carlson, A.E., Sinclair, G., DeConto, R.M., 2018.
- Greenland-Wide Seasonal Temperatures During the Last Deglaciation. Geophys. Res. Lett.
- 758 45, 1905–1914. https://doi.org/10.1002/2017GL075601
- 759 Cuzzone, J.K., Schlegel, N.-J., Morlighem, M., Larour, E., Briner, J.P., Seroussi, H., Caron, L.,
- 760 2019. The impact of model resolution on the simulated Holocene retreat of the
- southwestern Greenland ice sheet using the Ice Sheet System Model (ISSM). The
- 762 Cryosphere 13, 879–893. https://doi.org/10.5194/tc-13-879-2019
- 763 Cuzzone, J.K., Young, N.E., Morlighem, M., Briner, J.P., Schlegel, N.-J., 2022. Simulating the
- Holocene deglaciation across a marine-terminating portion of southwestern Greenland in
- response to marine and atmospheric forcings. The Cryosphere 16, 2355–2372.
- 766 https://doi.org/10.5194/tc-16-2355-2022
- Dangendorf, S., Frederikse, T., Chafik, L., Klinck, J.M., Ezer, T., Hamlington, B.D., 2021. Data-
- driven reconstruction reveals large-scale ocean circulation control on coastal sea level. Nat.
- 769 Clim. Change 11, 514–520. https://doi.org/10.1038/s41558-021-01046-1

- Downs, J., Johnson, J., Briner, J., Young, N., Lesnek, A., Cuzzone, J., 2020. Western Greenland
- ice sheet retreat history reveals elevated precipitation during the Holocene thermal
- 772 maximum. The Cryosphere 14, 1121–1137. https://doi.org/10.5194/tc-14-1121-2020
- 773 Dziewonski, A.M., Anderson, D.L., 1981. Preliminary reference Earth model. Phys. Earth Planet.
- 774 Inter. 25, 297–356. https://doi.org/10.1016/0031-9201(81)90046-7
- Fischer, H., Meissner, K.J., Mix, A.C., Abram, N.J., Austermann, J., Brovkin, V., Capron, E.,
- Colombaroli, D., Daniau, A.-L., Dyez, K.A., Felis, T., Finkelstein, S.A., Jaccard, S.L.,
- McClymont, E.L., Rovere, A., Sutter, J., Wolff, E.W., Affolter, S., Bakker, P., Ballesteros-
- Cánovas, J.A., Barbante, C., Caley, T., Carlson, A.E., Churakova, O., Cortese, G.,
- Cumming, B.F., Davis, B.A.S., de Vernal, A., Emile-Geay, J., Fritz, S.C., Gierz, P.,
- Gottschalk, J., Holloway, M.D., Joos, F., Kucera, M., Loutre, M.-F., Lunt, D.J., Marcisz,
- K., Marlon, J.R., Martinez, P., Masson-Delmotte, V., Nehrbass-Ahles, C., Otto-Bliesner,
- 782 B.L., Raible, C.C., Risebrobakken, B., Sánchez Goñi, M.F., Arrigo, J.S., Sarnthein, M.,
- Sjolte, J., Stocker, T.F., Velasquez Alvárez, P.A., Tinner, W., Valdes, P.J., Vogel, H.,
- Wanner, H., Yan, Q., Yu, Z., Ziegler, M., Zhou, L., 2018. Palaeoclimate constraints on the
- impact of 2 °C anthropogenic warming and beyond. Nat. Geosci. 11, 474–485.
- 786 https://doi.org/10.1038/s41561-018-0146-0
- 787 Fleming, K., Lambeck, K., 2004. Constraints on the Greenland Ice Sheet since the Last Glacial
- Maximum from sea-level observations and glacial-rebound models. Quat. Sci. Rev. 23,
- 789 1053–1077. https://doi.org/10.1016/j.quascirev.2003.11.001
- 790 Fox-Kemper, B., Hewitt, H.T., Xiao, C., Aðalgeirsdóttir, G., Drijfhout, S.S., Edwards, T.L.,
- Golledge, N.R., Hemer, M., Kopp, R.E., Krinner, G., Mix, A., Notz, D., Nowicki, S.,
- Nurhati, I.S., Ruiz, L., Sallée, J.-B., Slangen, A.B.A., Yu, Y., 2021. Ocean, cryosphere,

- and sea level change, in: Masson-Delmotte, V., Zhai, P., Pirani, A., Connors, S.L., Péan,
- C., Berger, S., Caud, N., Chen, Y., Goldfarb, L., Gomis, M.I., Huang, M., Leitzell, K.,
- Lonnoy, E., Matthews, J.B.R., Maycock, T.K., Waterfield, T., Yelekçi, Ö., Yu, R., Zhou,
- B. (Eds.), Climate Change 2021: The Physical Science Basis. Contribution of Working
- Group I to the Sixth Assessment Report of the Intergovernmental Panel on Climate
- 798 Change. Cambridge University Press, Cambridge, United Kingdom and New York, NY,
- 799 USA, pp. 1211–1362. https://doi.org/10.1017/9781009157896.001
- Fredskild, B., 1983. The Holocene development of some low and high arctic Greenland lakes.
- 801 Hydrobiologia 103, 217–224.
- 802 Kendall, R.A., Mitrovica, J.X., Milne, G.A., 2005. On post-glacial sea level II. Numerical
- formulation and comparative results on spherically symmetric models. Geophys. J. Int.
- 804 161, 679–706. https://doi.org/10.1111/j.1365-246X.2005.02553.x
- Khan, S.A., Sasgen, I., Bevis, M., van Dam, T., Bamber, J.L., Wahr, J., Willis, M., Kjær, K.H.,
- Wouters, B., Helm, V., Csatho, B., Fleming, K., Bjørk, A.A., Aschwanden, A., Knudsen,
- P., Munneke, P.K., 2016. Geodetic measurements reveal similarities between post–Last
- Glacial Maximum and present-day mass loss from the Greenland ice sheet. Sci. Adv. 2,
- e1600931. https://doi.org/10.1126/sciadv.1600931
- 810 Kobashi, T., Menviel, L., Jeltsch-Thömmes, A., Vinther, B.M., Box, J.E., Muscheler, R.,
- Nakaegawa, T., Pfister, P.L., Döring, M., Leuenberger, M., Wanner, H., Ohmura, A., 2017.
- Volcanic influence on centennial to millennial Holocene Greenland temperature change.
- 813 Sci. Rep. 7, 1441. https://doi.org/10.1038/s41598-017-01451-7
- Larsen, N.K., Kjær, K.H., Lecavalier, B., Bjørk, A.A., Colding, S., Huybrechts, P., Jakobsen, K.E.,
- Kjeldsen, K.K., Knudsen, K.-L., Odgaard, B.V., Olsen, J., 2015. The response of the

- southern Greenland ice sheet to the Holocene thermal maximum. Geology 43, 291–294.

 https://doi.org/10.1130/G36476.1

 Lea, J.M., Mair, D.W.F., Nick, F.M., Rea, B.R., Weidick, A., Kjær, K.H., Morlighem, M., Van
- As, D., Schofield, J.E., 2014. Terminus-driven retreat of a major southwest Greenland tidewater glacier during the early 19th century: insights from glacier reconstructions and
- numerical modelling. J. Glaciol. 60, 333–344. https://doi.org/10.3189/2014JoG13J163
- Lecavalier, B.S., Milne, G.A., Simpson, M.J.R., Wake, L., Huybrechts, P., Tarasov, L., Kjeldsen,
- K.K., Funder, S., Long, A.J., Woodroffe, S., Dyke, A.S., Larsen, N.K., 2014. A model of
- Greenland ice sheet deglaciation constrained by observations of relative sea level and ice
- extent. Quat. Sci. Rev. 102, 54–84. https://doi.org/10.1016/j.quascirev.2014.07.018
- Lesnek, A.J., Briner, J.P., Young, N.E., Cuzzone, J.K., 2020. Maximum Southwest Greenland Ice
- Sheet Recession in the Early Holocene. Geophys. Res. Lett. 47, 1–11
- https://doi.org/10.1029/2019GL083164
- 829 Levitus, S., Antonov, J.I., Boyer, T.P., Baranova, O.K., Garcia, H.E., Locarnini, R.A., Mishonov,
- A.V., Reagan, J.R., Seidov, D., Yarosh, E.S., Zweng, M.M., 2012. World ocean heat
- content and thermosteric sea level change (0–2000 m), 1955–2010. Geophys. Res. Lett.
- 39, L10603. https://doi.org/10.1029/2012GL051106
- 833 Liu, Z., Otto-Bliesner, B.L., He, F., Brady, E.C., Tomas, R., Clark, P.U., Carlson, A.E., Lynch-
- Stieglitz, J., Curry, W., Brook, E., Erickson, D., Jacob, R., Kutzbach, J., Cheng, J., 2009.
- Transient Simulation of Last Deglacation with a New Mechanism for Bølling-Allerød
- Warming. Science, 325, 310-314. https://doi.org/10.1126/science.1171041
- 837 Long, A.J., Woodroffe, S.A., Roberts, D.H., Dawson, S., 2011. Isolation basins, sea-level changes
- and the Holocene history of the Greenland Ice Sheet. Quat. Sci. Rev. 30, 3748–3768.

- https://doi.org/10.1016/j.quascirev.2011.10.013
- Mouginot, J., Rignot, E., Bjørk, A.A., van den Broeke, M., Millan, R., Morlighem, M., Noël, B.,
- Scheuchl, B., Wood, M., 2019. Forty-six years of Greenland Ice Sheet mass balance from
- 842 1972 to 2018. Proc. Natl. Acad. Sci. 116, 9239–9244.
- https://doi.org/10.1073/pnas.1904242116
- Paxman, G.J.G., Lau, H.C.P., Austermann, J., Holtzman, B.K., Havlin, C., 2023. Inference of the
- Timescale-Dependent Apparent Viscosity Structure in the Upper Mantle Beneath
- Greenland. AGU Adv. 4, e2022AV000751. https://doi.org/10.1029/2022AV000751
- Pearce, D.M., Lea, J.M., Mair, D.W.F., Rea, B.R., Schofield, J.E., Kamenos, N.A., Schoenrock,
- K.M., Stachnik, L., Lewis, B., Barr, I., Mottram, R., 2022. Greenland tidewater glacier
- advanced rapidly during era of Norse settlement. Geology 50, 704–709.
- 850 https://doi.org/10.1130/G49644.1
- Peltier, W.R., Argus, D.F., Drummond, R., 2015. Space geodesy constrains ice age terminal
- deglaciation: The global ICE-6G_C (VM5a) model: Global Glacial Isostatic Adjustment.
- J. Geophys. Res. Solid Earth 120, 450–487. https://doi.org/10.1002/2014JB011176
- Peltier, W.R., Fairbanks, R.G., 2006. Global glacial ice volume and Last Glacial Maximum
- duration from an extended Barbados sea level record. Quat. Sci. Rev. 25, 3322–3337.
- https://doi.org/10.1016/j.quascirev.2006.04.010
- 857 Rantanen, M., Karpechko, A.Yu., Lipponen, A., Nordling, K., Hyvärinen, O., Ruosteenoja, K.,
- Vihma, T., Laaksonen, A., 2022. The Arctic has warmed nearly four times faster than the
- globe since 1979. Commun. Earth Environ. 3, 168. https://doi.org/10.1038/s43247-022-
- 860 00498-3
- Richards, F.D., Hoggard, M.J., White, N., Ghelichkhan, S., 2020. Quantifying the Relationship

- Between Short-Wavelength Dynamic Topography and Thermomechanical Structure of the
 Upper Mantle Using Calibrated Parameterization of Anelasticity. J. Geophys. Res. Solid
- Earth 125. https://doi.org/10.1029/2019JB019062
- 865 Roy, K., Peltier, W.R., 2017. Space-geodetic and water level gauge constraints on continental
- uplift and tilting over North America: regional convergence of the ICE-6G_C
- 867 (VM5a/VM6) models. Geophys. J. Int. 210, 1115–1142.
- 868 https://doi.org/10.1093/gji/ggx156
- 869 Schaeffer, A.J., Lebedev, S., 2014. Imaging the North American continent using waveform
- inversion of global and USArray data. Earth Planet. Sci. Lett. 402, 26–41.
- https://doi.org/10.1016/j.epsl.2014.05.014
- 872 Serreze, M.C., Francis, J.A., 2006. The Arctic Amplification Debate. Clim. Change 76, 241–264.
- 873 https://doi.org/10.1007/s10584-005-9017-y
- 874 Simon, K. M., Riva, R. E. M., & Broerse, T. (2022). Identifying geographical patterns of transient
- deformation in the geological sea level record. Journal of Geophysical Research: Solid
- 876 Earth, 127, e2021JB023693. https://doi.org/10.1029/2021JB023693
- Slangen, A.B.A., 2012. Modelling regional sea-level changes in recent past and future.
- 878 Solomon, S., Intergovernmental Panel on Climate Change, Intergovernmental Panel on Climate
- Change (Eds.), 2007. Climate change 2007: The Physical Science Basis: Contribution of
- Working Group I to the Fourth Assessment Report of the Intergovernmental Panel on
- Climate Change. Cambridge University Press, Cambridge; New York.
- Spada, G., Galassi, G., Olivieri, M., 2014. A study of the longest tide gauge sea-level record in
- Greenland (Nuuk/Godthab, 1958–2002). Glob. Planet. Change 118, 42–51.
- https://doi.org/10.1016/j.gloplacha.2014.04.001
- Spada, G., Stocchi, P., 2007. SELEN: A Fortran 90 program for solving the "sea-level equation."

886 Comput. Geosci. 33, 538–562. https://doi.org/10.1016/j.cageo.2006.08.006 887 Stuhne, G.R., Peltier, W.R., 2015. Reconciling the ICE-6G_C reconstruction of glacial chronology 888 with ice sheet dynamics: The cases of Greenland and Antarctica: ICE-6G C and ICE-Sheet 889 Dynamics. J. Geophys. Surf. 120, Res. Earth 1841–1865. 890 https://doi.org/10.1002/2015JF003580 Tarasov, L., Dyke, A.S., Neal, R.M., Peltier, W.R., 2012. A data-calibrated distribution of 891 892 deglacial chronologies for the North American ice complex from glaciological modeling. 893 Earth Planet. Sci. Lett. 315–316, 30–40. https://doi.org/10.1016/j.epsl.2011.09.010 894 Tarasov, L., Peltier, W.R., 2003. Greenland glacial history, borehole constraints, and Eemian 895 extent: GREENLAND GLACIAL HISTORY. J. Geophys. Res. Solid Earth 108. 896 https://doi.org/10.1029/2001JB001731 897 Tarasov, L., Peltier, W.R., 2002. Greenland glacial history and local geodynamic consequences. 898 Geophys. J. Int. 150, 198–229. https://doi.org/10.1046/j.1365-246X.2002.01702.x 899 Weidick, A., 1974. Investigations on the Quaternary deposits in the Fiskenæsset region, southern 900 West Greenland. Grønl. Geol. Unders. 65, 65–65. Rapp. 901 https://doi.org/10.34194/rapggu.v65.7391 902 Weidick, A., Bennike, O., 2007. Quaternary glaciation history and glaciology of Jakobshavn Isbræ 903 and the Disko Bugt region, West Greenland: a review. Geol. Surv. Den. Greenl. Bull. 14, 904 1–78. https://doi.org/10.34194/geusb.v14.4985 905 Weidick, A., Bennike, O., Citterio, M., Nørgaard-Pedersen, N., 2012. Neoglacial and historical 906 glacier changes around Kangersuneq fjord in southern West Greenland. Geol. Surv. Den. 907 Greenl. Bull. 27, 1–68. https://doi.org/10.34194/geusb.v27.4694 908 Young, N.E., Briner, J.P., 2015. Holocene evolution of the western Greenland Ice Sheet: Assessing

909	geophysical ice-sheet models with geological reconstructions of ice-margin change. Quat.
910	Sci. Rev. 114, 1–17. https://doi.org/10.1016/j.quascirev.2015.01.018
911	Young, N.E., Briner, J.P., Miller, G.H., Lesnek, A.J., Crump, S.E., Thomas, E.K., Pendleton, S.L.,
912	Cuzzone, J., Lamp, J., Zimmerman, S., Caffee, M., Schaefer, J.M., 2020. Deglaciation of
913	the Greenland and Laurentide ice sheets interrupted by glacier advance during abrupt
914	coolings. Quat. Sci. Rev. 229, 106091. https://doi.org/10.1016/j.quascirev.2019.106091
915	Young, N.E., Lesnek, A.J., Cuzzone, J.K., Briner, J.P., Badgeley, J.A., Balter-Kennedy, A.,
916	Graham, B.L., Cluett, A., Lamp, J.L., Schwartz, R., Tuna, T., Bard, E., Caffee, M.W.,
917	Zimmerman, S.R.H., Schaefer, J.M., 2021. In situ cosmogenic 10Be-14C-26 Al
918	measurements from recently deglaciated bedrock as a new tool to decipher changes in
919	Greenland Ice Sheet size. Clim. Past 17, 419–450. https://doi.org/10.5194/cp-17-419-2021